ANALYSIS OF THE LEARJET 35/36 WING AND CORRELATION WITH EXPERIMENTAL RESULTS

Mike H. Abla and Robert R. Boroughs
Gates Learjet Corporation

Everett L. Cook
Wichita State University

SUMMARY

Two NASTRAN models of the Gates Learjet Corporation Model 35/36 Wing have been developed. This paper describes the models and discusses the problems encountered in their development. A skin buckling analysis used for the ultimate loading conditions is presented. A discussion of the static tests and the correlation of the static test with the NASTRAN results and the results of a supplementary semimonocoque beam analysis are also included.

INTRODUCTION

The purpose of the investigation described herein is to develop an accurate finite element model of the Gates Learjet Corporation (GLC) Model 35/36 wing. This wing is an 8-spar wet wing with large external fuel tanks at the tips (fig. 1). It is continuous from tip to tip with all loads transferred to the fuselage through four fittings on each side. It is a derivative of previous GLC wings, with the most noticeable difference being the wing tip extensions. There are also internal structural modifications which were incorporated to accommodate the increased gross weight of the Model 35/36.

An in-house finite element program, based on reference 1, was used during the design and certification testing of the wing. This program has severe time and space limitations; therefore, the decision was made to acquire and implement NASTRAN. The prior experience with modeling the wing, plus the extensive experimental dtat available from the static tests, resulted in the decision to develop a new wing model to demonstrate the capabilities of NASTRAN.

SYMBOLS

Values are given in both SI and U.S. Customary Units. The measurements and calculations were made in U.S. Customary Units.

b	width of a skin panel, cm (in.)
b'	reduced width of a skin panel, cm (in.)
C	constant = b'/2b
E	Young's modulus, N/M^2 (psi)

$F_{c_{cr}}$	buckling stress of a skin panel, N/m^2 (psi)
F_{st}	allowable stress of a spar cap, N/m^2 (psi)
f	local stress in a skin panel, N/m^2 (psi)
f_{st}	actual stress in a spar cap, N/m^2 (psi)
P	total load carried by one-half of a skin panel, N (lb)
t	actual thickness of a skin panel, cm (in.)
t_e	effective thickness of a skin panel, cm (in.)
w	effective width of skin acting with a spar cap at failure, cm (in.)
x	distance from centerline of spar cap to point where local stress is measured, cm (in.)

NASTRAN MODELS

Two NASTRAN models were generated and analyzed. The first model, called the Demonstration Model, has a relatively coarse grid pattern and was used to gain experience with NASTRAN at a reasonable cost. It was not expected that the results obtained from this model would be satisfactory for comparison with the experimental data. The final model, called the Refined Model, is a much more accurate model of the wing. Some of the results of the analysis of the Refined Model are subsequently compared with the experimental data.

The wing structure is symmetrical with respect to the centerline of the airplane; therefore, only the left wing is modeled.

The Demonstration Model

The grid points for the primary wing structure were selected at the spar cap-rib cap intersections (fig. 2). Except for Spar 6, the spars are continuous from tip-to-tip, although there are changes in sweep angles at some of the ribs. Spar 6 only extends from the landing gear rib outboard. The ribs are continuous from the front to the rear spar and are parallel to the airplane centerline, except for the fuselage attach rib which does not extend through the wheel well. This rib is also not straight in order that the attachment fittings may be properly aligned with the fuselage fittings. Thus, the primary structure is defined by 126 grid points. The leading edge, which extends from the landing gear rib to the tip, is defined by four rows of grid points forward of Spar 1; and a simulated tip tank is defined by an additional ten grid points. Therefore, this model has a total of 160 grid points.

The skins from the centerline of the airplane to the wing tip extension rib are machine sculptured. The upper skin tapers, while the lower skin is of constant thickness. The leading edge and the skins on the wing extension are standard aluminum sheet. The NASTRAN element used to model the skins and the leading edge is the QDMEM1 isoparametric quadrilateral membrane. This element was chosen because it does not overestimate the stiffness as much as the other two quadrilateral membranes (ref. 2). There are no skin elements in the wheel well region on either surface; although on the actual wing, the upper wheel well cutout only extends outboard to the fuselage attach rib.

The spars are a combination of formed channels and built-up channels and I-sections, with most of the formed sections in the outboard wing and most of the built-up sections inboard. The spar webs are modeled with SHEAR elements and the spar caps with ROD elements. The cap areas include not only the actual cap areas, but also the areas of the lands in the sculptured skin and the effective area of the spar webs. The ribs are also modeled with SHEAR's for the webs and ROD's for the caps. The only other internal structure in this model, the vertical stiffeners on the spars, are modeled with ROD's.

Since loads were applied to the tip tank during the static test, a simulated tip tank is included in the model. A series of nodes along the centerline of the tank are connected together by very stiff BAR elements. These nodes are then connected to the outboard ends of the spars with a series of ROD elements.

All of the grid points, except those on the tip tank, are constrained against rotation. The only other constraints are at the root rib and at the fuselage attach rib. Due to the symmetry of both the structure and the loadings, all of the grid points at the centerline of the airplane are constrained in the spanwise direction. They are free, however, to translate in the other two coordinate directions. The fuselage fittings on the fuselage attach rib extend upward from the upper surface at Spars 2, 5, 7 and 8. Due to the complexity of these fittings and their matching fittings on the fuselage, no attempt was made to model them; so the constraints are applied at the corresponding upper surface grid points. The main fitting at Spar 5 is assumed to be constrained in the vertical and chordwise directions, while the others are constrained only in the vertical direction.

The Refined Model

All of the grid points in the Demonstration Model are included in the Refined Model. Chordwise rows of grid points were added between the ribs to form approximately square skin panels (fig. 3). Figure 4 shows the details of a typical spanwise section between two ribs. Additional grid points were also added in order to be able to model the diagonal redistribution stringers that transfer the loads from Spar 6 to Spars 5 and 7 just outboard of the wheel well cutouts. This resulted in a total of 538 grid points for the model.

The first version of the Refined Model had the same basic elements as the Demonstration Model: QDMEM1's for the skins, SHEAR's for the spar and rib webs and ROD's for the spar and rib caps and spar stiffners. However, problems developed with the QDMEM1 skin elements. Since all of the ribs outboard of the fuselage attach rib are parallel, the skin elements are very nearly trapezoids, and in the wing tip extension are very nearly parallelograms. This geometry apparently caused a near-singularity in the generation of the element stiffness and/or stress matrices, because the calculated stresses for some of the elements were obviously erroneous. It has been shown (refs. 2 and 3) that singularities do occur when a general gradrilateral approaches a more regular shape, such as a trapezoid or parallelogram. NSMO was contacted regarding the problem. They were able to duplicate our results on the IBM version of NASTRAN, but not on the CDC version, and found that the problem could be eliminated by rotating the node numbering sequence 90 degrees (ref. 4). Rather than reordering the nodes, it was decided to model all of the quadrilateral membranes with QDMEM2 elements, and no further problems have been encountered.

The most important new members included in the Refined Model are the splice plates and the stringers between the spars. In addition to the diagonal redistribution stringers, there are spanwise stringers between the spar caps throughout the inboard portion of the wing. To avoid adding more grid points, ROD elements were added in parallel with the spar cap elements to effectively add the stringer areas to the spar cap areas. Another problem associated with these stringers is due to the fact that their main function is to increase the buckling stresses of the skin panels, so they are not continuous across all of the ribs. This causes stress concentrations in the skins at these ribs that are difficult to reproduce in the finite element analysis. This effect is approximately accounted for by reducing the stringer areas near their ends. The splice plates at the wing root were handled in essentially the same way as the stringers; QDMEM2 elements were added in parallel with the appropriate skin elements. The addition of the redistribution stringers necessitated the use of some TRMEM elements in the upper and lower skins (fig. 3). It was also necessary to introduce dummy ROD elements to support the upper skin over the wheel well.

Another important consideration in the Refined Model are the access doors in the lower skin. These doors cover cutouts that are used during the assembly of the wing and later provide access to the fuel tanks and the control systems. To provide easy access and interchangeability, the doors are attached by means of screws and nut plates through medium tolerance holes. As a result, they are not fully effective, and a study of the strain gage data revealed that their effectiveness is different in tension and compression. The values selected for the final analyses were 35 percent effectiveness for tension and 72 percent for compression. These values were used to calculate the effective thickness of the skin elements affected.

The initial limit load analyses after the skin elements were changed to QDMEM2's produced acceptable results outboard of the landing gear rib, but not inboard. Both skins are extensively sculptured in the inboard region, plus the lower skin has several small cutouts. Therefore, an integration scheme was used

to redefine the effective skin thicknesses. This resulted in a marked improvement in the calculated deflections and stresses, but more work needs to be done to accurately model this complex region of the structure.

The constraints are the same for both the Demonstration and Refined Models. The tip tank models are also the same, although figure 3 shows a new, more accurate tip tank model that is being developed.

LOADS AND THE STATIC TEST

The primary purpose of the analysis reported here is to provide a comparison of the NASTRAN results with the static test results. Therefore the loads used with the NASTRAN data were derived from the static test loads.

Eight symmetric loading conditions were included in the static test program. These include fuel tank integrity tests and fail safe tests as well as strength tests. Three of these loading conditions were selected for the NASTRAN analysis: limit positive bending, ultimate positive bending and ultimate negative bending.

The test article was a complete airplane, with the loads applied to the wing and tip tank and reacted by the fuselage. Hydraulic actuators were used to apply the loads, through whiffle tree systems, to tension patches on the wing and straps riveted to the tip tanks. Figures 5 and 6 show the test set-up for positive and negative bending, respectively.

The tension patch loads were "beamed" to the grid points at the adjacent ribs. Grid points were located at the load points on the tip tank, so no transfer of load was required. The loads are identical for both the Demonstration and Refined Models.

Two hundred channels of strain gage and deflection transducer data were recorded for each test. Originally, there were 114 strain gages on the outer surface of the left wing and 9 gages on the spar caps in the wing. They were arranged in both spanwise and chordwise rows so that an excellent picture of the strain distribution was obtained. Several gages were destroyed in a local failure during an early test, but these gages were replaced by corresponding gages on the right wing. Of course, there were other gage failures prior to the destruction test, but there was still sufficient data for a good comparison with the ultimate positive bending NASTRAN analysis.

BUCKLING ANALYSIS

In the usual wing strength analysis, there are two primary criteria: there shall be no detrimental permanent set at limit loads, and the structure shall not fail at ultimate loads. The limit load strength analysis is generally

limited to showing that any skin panels that buckle do so elastically, rather than plastically. For the ultimate load analysis, the major concern is the calculation of the allowable bending moments at the critical cross sections, so they can be compared with the actual bending moments. Since the compression skins are usually buckled at failure, it is customary to replace the buckled skin with effective widths of skin acting with the compression stringers. The effective width is given by the equation (refs. 5 and 6):

$$w = 1.7t\sqrt{\frac{E}{F_{st}}} \tag{1}$$

The purpose of this analysis, however, was not to predict the failing loads; but to compare analytical and experimental deflections and stresses at specified loads. Therefore, a method was needed for calculating the effective skin at stresses between the skin buckling stress and the spar cap buckling stress. Figure 7 shows the assumed post-buckling stress distribution. The stress adjacent to the spar cap is a cosine distribution and is given by

$$f = \frac{f_{st} + F_{c_{cr}}}{2} + \frac{f_{st} - F_{c_{cr}}}{2} \cos \frac{2\pi x}{b'} \quad \left(0 \le x \le \frac{b'}{2}\right) \tag{2}$$

while the stress in the center of the panel is

$$f = F_{c_{cr}} \quad \left(\frac{b'}{2} \le x \le \frac{b}{2}\right) \tag{3}$$

The total load represented by this stress distribution is the area under the curve times the thickness, or

$$P = \left[\frac{b}{2} F_{c_{cr}} + \frac{b'}{2} \left(\frac{f_{st} - F_{c_{cr}}}{2}\right)\right] t \tag{4}$$

The distance b'/2 is determined by requiring that in the limiting case of $f_{st} = F_{st}$, the total load be equal to

$$P = \frac{w}{2} F_{st}\, t \tag{5}$$

Equating equations (4) and (5) gives

$$\frac{b'}{2} = \frac{w F_{st} - b F_{c_{cr}}}{F_{st} - F_{c_{cr}}} \tag{6}$$

For a finite element analysis with membrane elements for the skins, it is more convenient to use an effective thickness, instead of an effective width. This thickness can be defined by requiring the total load at the specified stringer stress to be

$$P = \frac{b}{2} f_{st} t_e \tag{7}$$

Then by equating equations (4) and (7)

$$\frac{t_e}{t} = C + (1 - C) \frac{F_{c_{cr}}}{f_{st}} \tag{8}$$

Note that since $t_e/t = 1$ when $f_{st} = F_{c_{cr}}$ and $b'/2$ was defined to give the standard effective width at failure, equation (8) provides an approximate method of interpolating between the limiting cases of skin buckling and stringer failure. At stresses below the buckling stress, the skin is assumed to be fully effective.

There were a few buckled skin panels at limit positive bending, but a buckling analysis was not performed for this loading condition. In fact, the primary reason for including limit positive bending was to obtain good analytical-experimental correlation prior to incorporating the buckling analysis. There was extensive buckling for the other two loading conditions, however; and reasonable correlation could not be achieved without including this nonlinear effect. Because of the nonlinearities, an iterative procedure was required. The stresses were first calculated, and punched, assuming that the skins were fully effective. A special program was then used to determine which panels were buckled and to calculate, and punch, effective skin thicknesses for these panels. This procedure was repeated, usually 4 or 5 iterations were necessary, until convergency was obtained.

There are two parameters in equations (1), (6) and (8) that must be specified: the spar cap allowable, F_{st}, and the skin buckling stress $F_{c_{cr}}$. In all cases the spar cap allowable was taken as the crippling stress, since the spar caps are stabilized against column buckling by the skin and spar webs. The skin buckling stresses were more of a problem. After considerable

experimentation, the panels inboard of the landing gear rib were assumed to be fully clamped, while those in the outboard wing were assumed to have edge conditions intermediate between clamped and simply supported.

SEMIMONOCOQUE BEAM ANALYSIS

The NASTRAN analysis was supplemented by a semimonocoque beam analysis for the ultimate positive bending condition. The analysis was performed using a program, SEMOBEAM, based on the displacement method (ref. 7). The spanwise stations at which the spar cap stresses were calculated corresponded to the NASTRAN grid point locations, except at the fuselage attach rib. Here, a dummy rib, parallel to the other ribs, was used.

The spar cap areas and web thicknesses used in the NASTRAN analysis are the average values in the bay between grid point lines. For the semimonocoque beam analysis these values were assumed to be those at the inboard end of the bay, i.e., at the inboard station. Since both the spar cap areas and the thicknesses generally increase from tip to root, this assumption will give slightly conservative results.

Several other modifications of the NASTRAN model were required for the SEMOBEAM model. These include:

1. Adding the axial load carrying capability of the skins to the spar cap areas. Since the thickness of any buckled panels had already been reduced in the NASTRAN model, all skins were assumed to be fully effective.

2. Adding dummy web elements in the wheel well region. Since the semimonocoque beam analysis used is valid only for beams with closed cells, the upper and lower skins and the web in Spar 6 were assumed to have a thickness of 0.001 inch.

3. Allocating the areas of the diagonal redistribution members to the adjacant spar caps.

4. Reducing the spar cap areas of Spar 6 at, and outboard of, the wheel well cutout to approximately account for shear lag effects. The areas of the leading edge stringers were also modified at, and outboard of, their inboard ends for the same reason.

The last three of the modifications described above are all in the root region of the wing where the results of the semimonocoque beam analysis are not expected to be accurate.

COMPARISON OF RESULTS

The correlation between the analytical and experimental results is good for all three loading conditions, with the best correlation being for the limit positive bending condition. The correlation is generally better outboard of the landing gear rib for all three loading conditions.

Sample plots from the ultimate positive bending analysis are shown in figures 8 to 11. Figure 8 shows the deflection of the front spar versus wing station. Although there were deflection scales on the inboard wing, they were not read above limit load; so that the only data shown is from the deflection transducers at the centerline and near the tips. The calculated deflections at the wing tips are somewhat less than the experimental values, as would be expected, because the finite element model is stiffer than the actual structure.

Figure 9 shows the strains in the upper skin approximately midway between Spars 4 and 5, where Spar 5 is the spar just forward of the wheel well. Strains are plotted, instead of stresses, because all of the experimental data is from axial strain gages, so that the Poisson's ratio effects are unknown. Thus, it is much more accurate to convert the calculated stresses to strains. The correlation for gages 90, 25, 140 and 143 is very good. Gages 135 and 147 are both on buckled panels, so they are not expected to show good correlation. Gage 22 shows an example of the stress concentration in the skin due to a stringer discontinuity across the landing gear rib.

Figures 10 and 11 show the upper and lower spar cap strains in Spars 3 and 5, respectively. In addition to the NASTRAN and experimental strains, the results of the SEMOBEAM analysis are shown in these figures. The NASTRAN/experimental correlation is good, with the calculated strains being generally conservative. Note that where there are two experimental values at a wing station, they represent back-to-back gages. The agreement between the NASTRAN and SEMOBEAM results is good outboard of the landing gear rib, but gets poorer as the root is approached.

CONCLUSIONS

The objective of the investigation is essentially accomplished. The Refined Model is considered to be an accurate finite element model of the GLC Model 35/36 wing; however, additional improvements are being made.

The complexity of this wing, particularly the sculptured skin and the access doors, created severe modeling problems. The availability of excellent strain gage data helped solve these problems and provided valuable modeling experience for future applications. The experimental data was also used as a guide in determining the edge conditions of the skin panels for the buckling analysis.

The only major NASTRAN related problem was the failure of the QDMEM1 element. Both the stresses and the deflections would probably have been more accurately calculated if this element could have been used for the skins.

It was not expected that the agreement between the finite element and semimonocoque beam analyses would be as good as they are in the outboard wing. These results indicate the semimonocoque beam analysis, coupled with the buckling analysis, would be adequate for design. This would allow a more detailed finite element model of the inboard wing.

REFERENCES

1. Abla, M.H.: Structural Analysis of Substructures Using Component Direct Stiffness Synthesis. M.S. Thesis, Wichita State University, February 1969.

2. Adelman, H.M.; Walz, J.E.; and Rogers, J.L.: An Isoparametric Quadrilateral Membrane Element for NASTRAN. NASTRAN: Users' Experiences, NASA TM X-2637, 1972, pp. 315 - 336.

3. Radovanov, M.N.: Quadrilateral Plate in Plane Stress. M.S. Thesis, Wichita State University, May 1970.

4. NASTRAN NEWSLETTER, Number 10 - August 22, 1975.

5. Bruhn, E.F.: Analysis and Design of Flight Vehicle Structures. Tri-State Offset, 1973 (pp. C7.10-11).

6. Peery, D.J.: Aircraft Structures, McGraw-Hill, 1950 (pp. 371 - 375).

7. Cook, E.L.: Semimonocoque Beam Analysis - A Displacement Formulation. SAE Paper 740385, April 1974.

FIGURE 1. LEARJET MODEL 35/36 AIRCRAFT

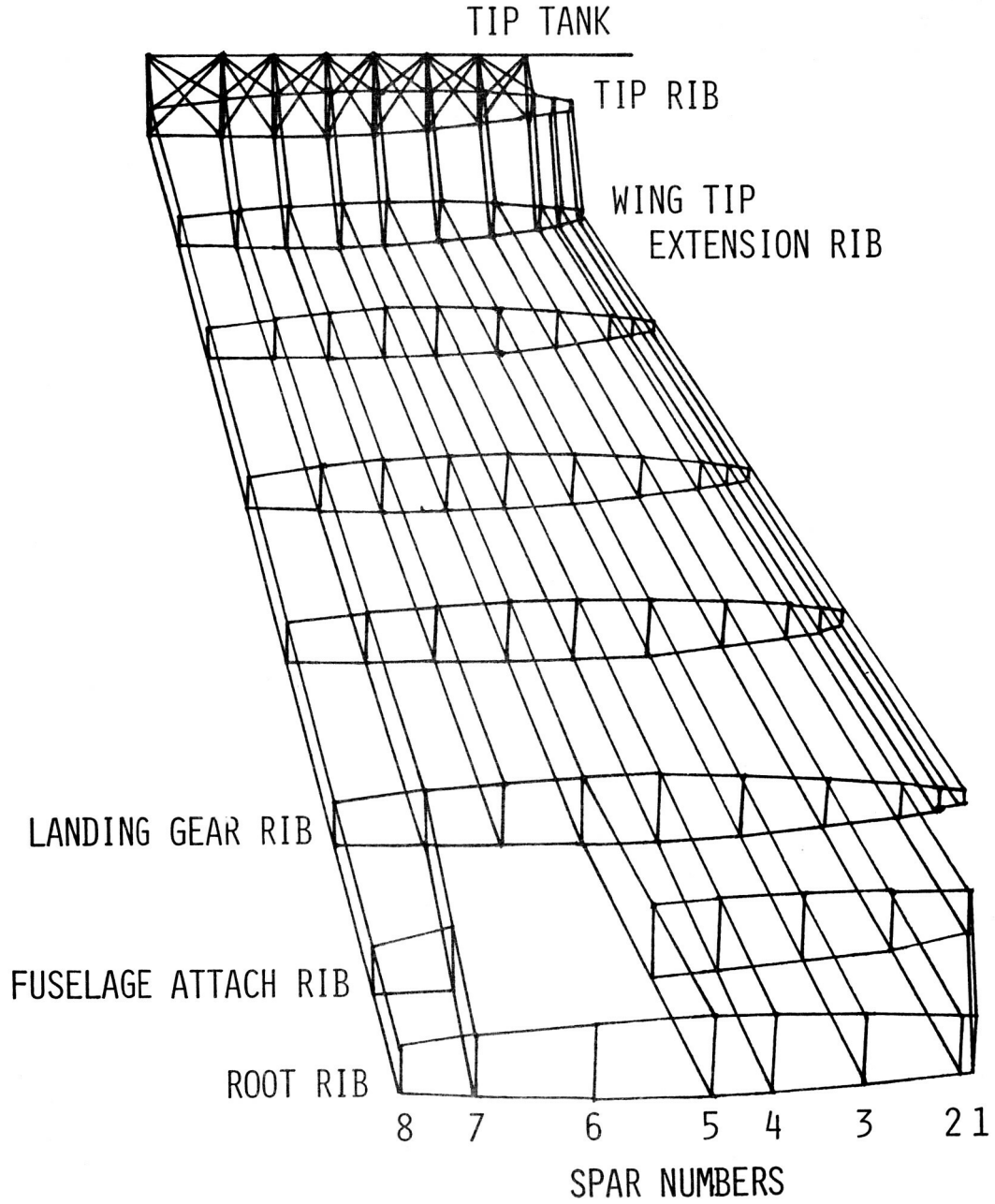

FIGURE 2. DEMONSTRATION MODEL

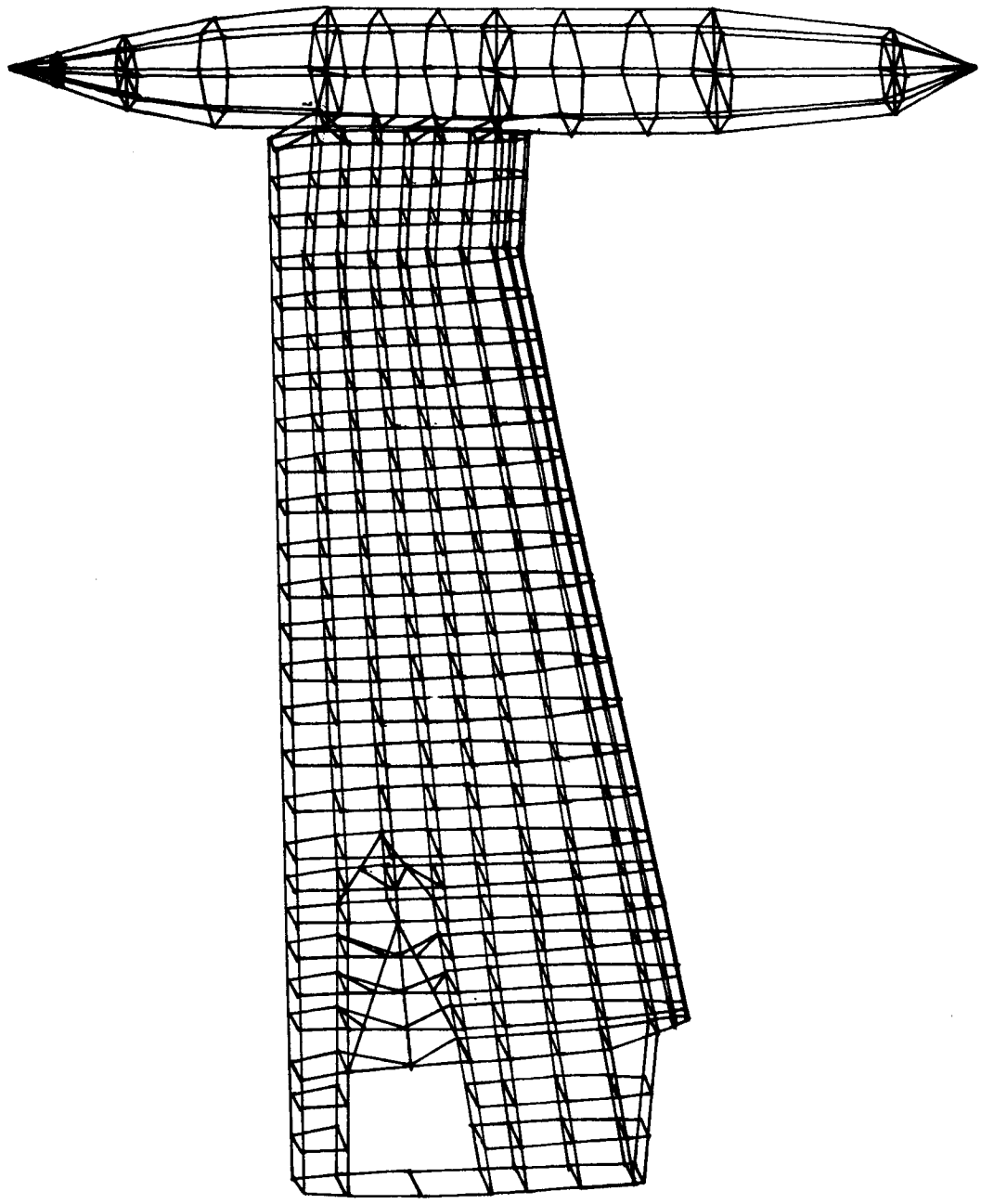

FIGURE 3. REFINED MODEL

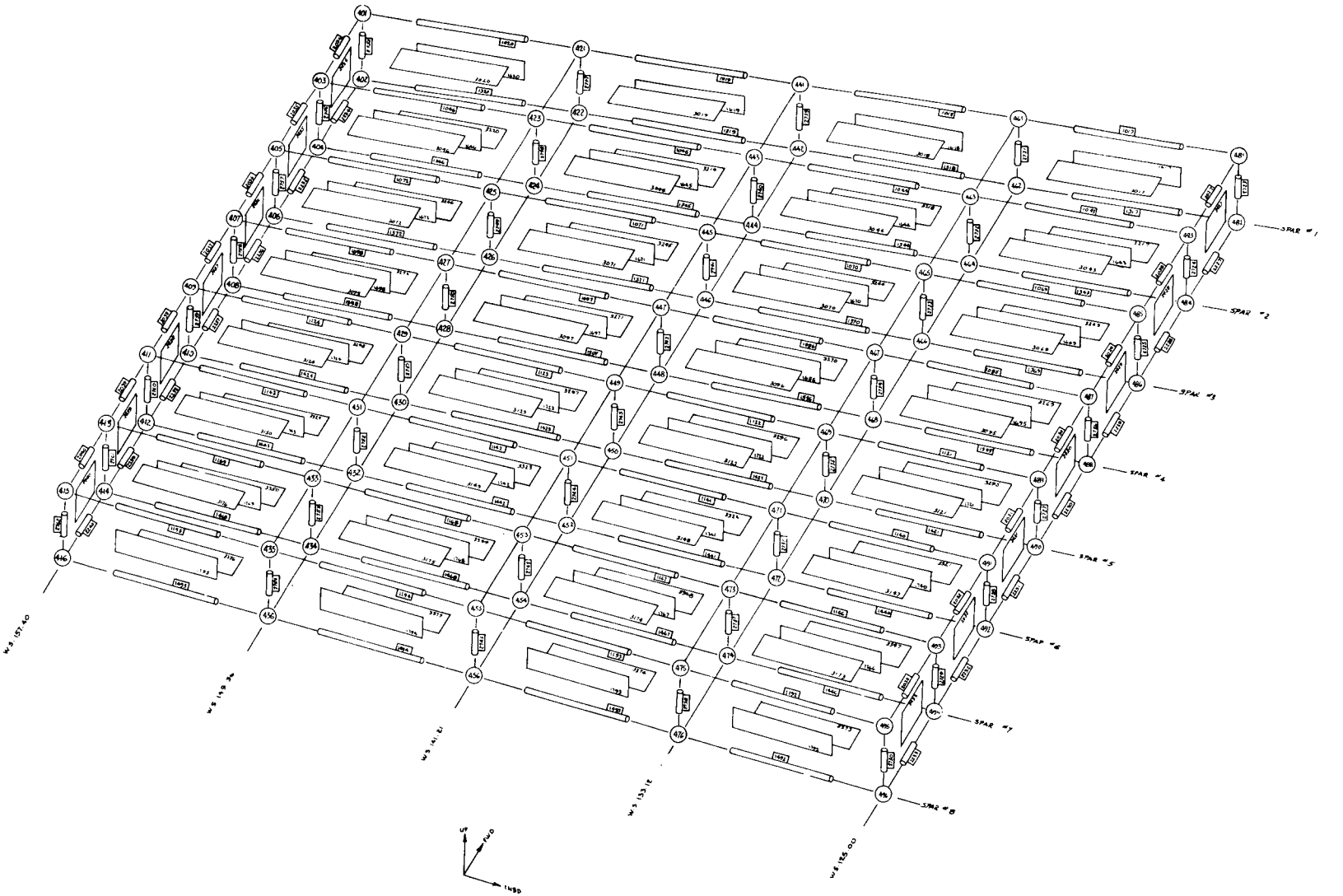

FIGURE 4. DETAILS OF THE REFINED MODEL

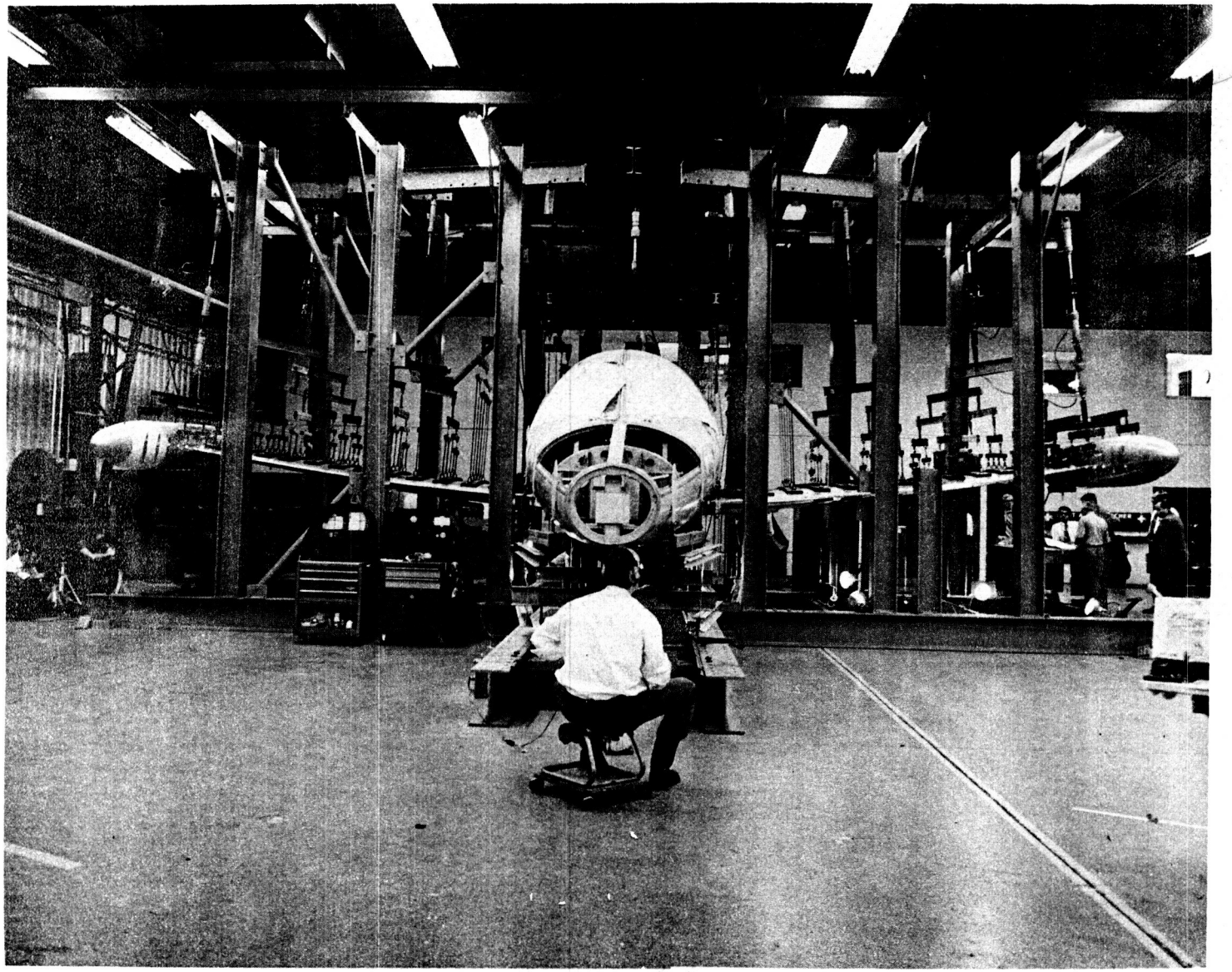

FIGURE 5. POSITIVE BENDING

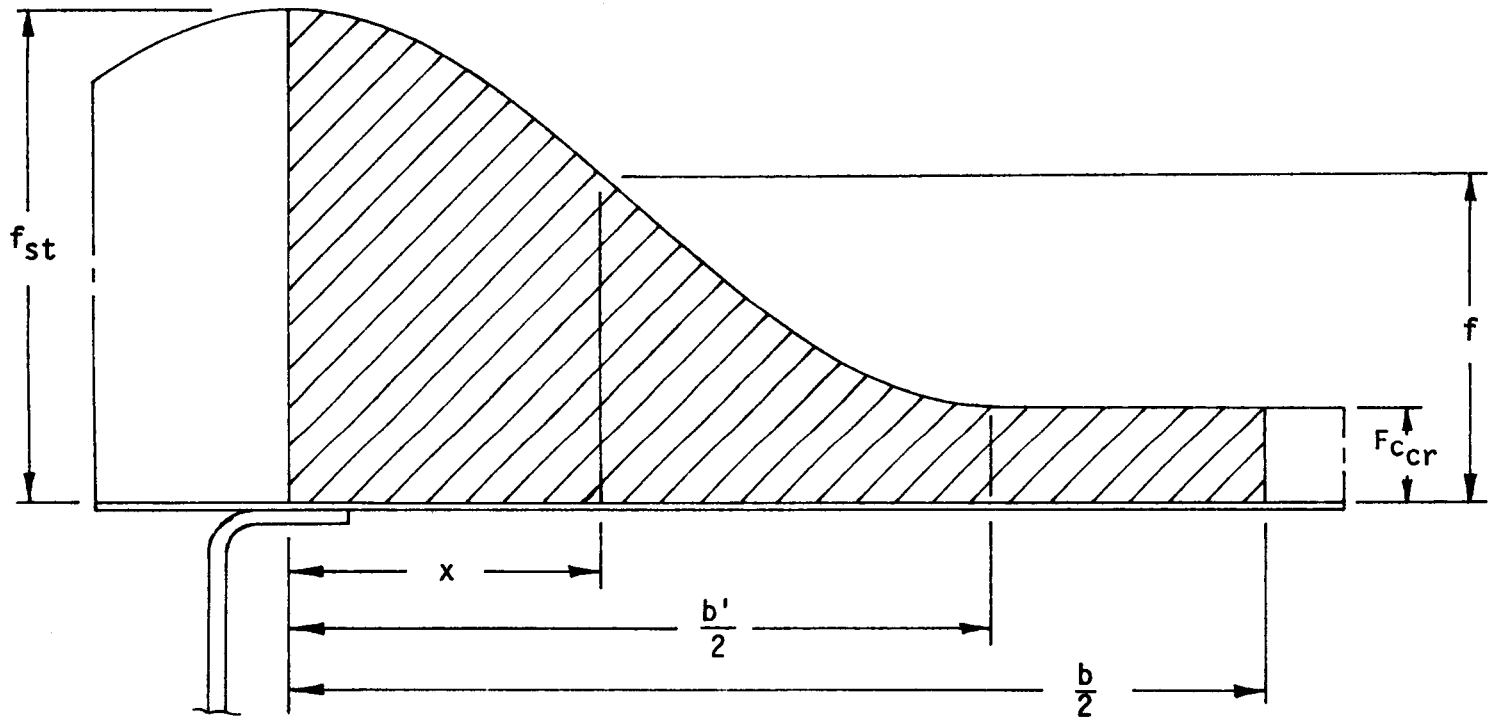

FIGURE 7. BUCKLED SKIN STRESS DISTRIBUTION

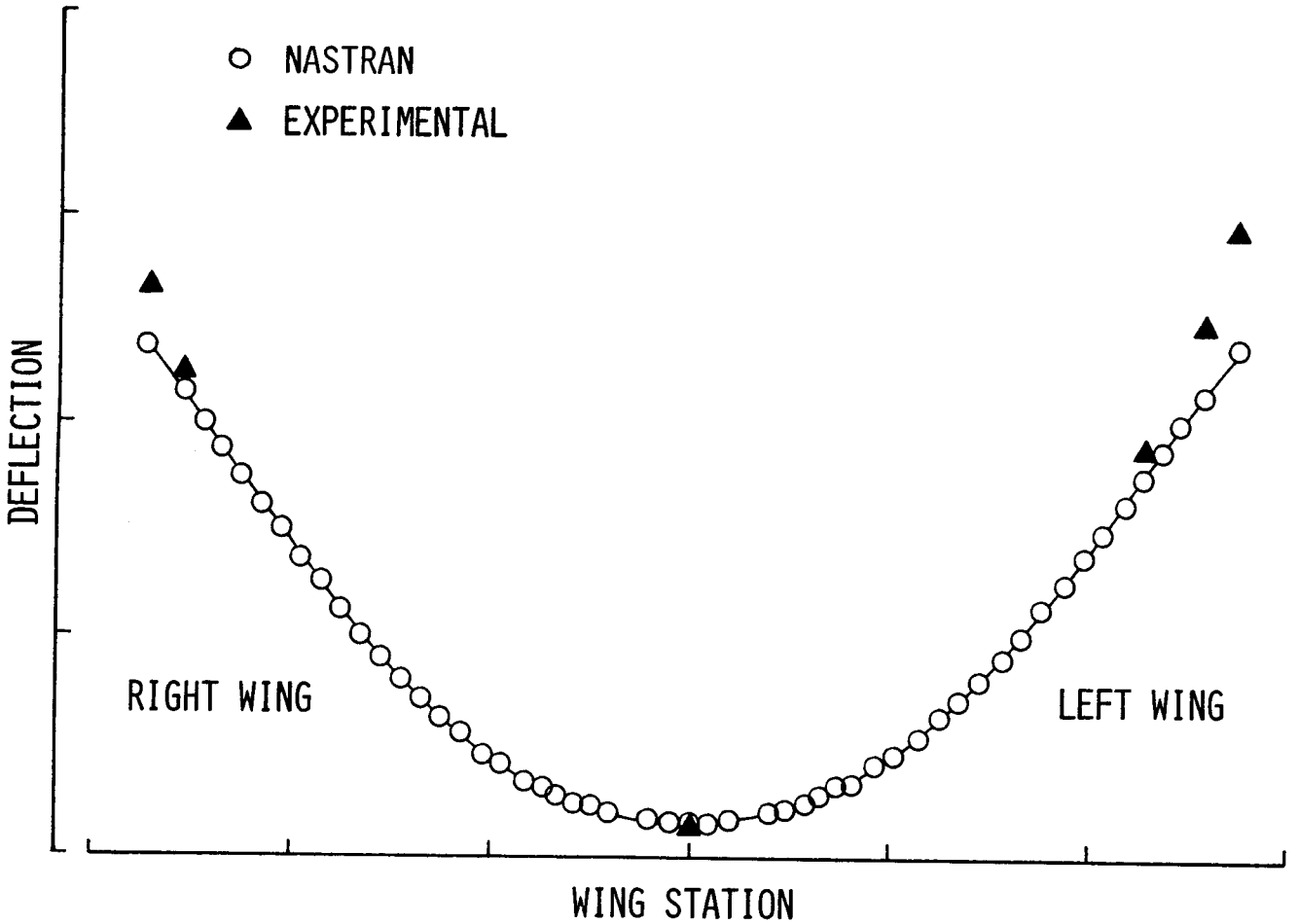

FIGURE 8. DEFLECTION OF SPAR 1 AT ULTIMATE POSITIVE BENDING

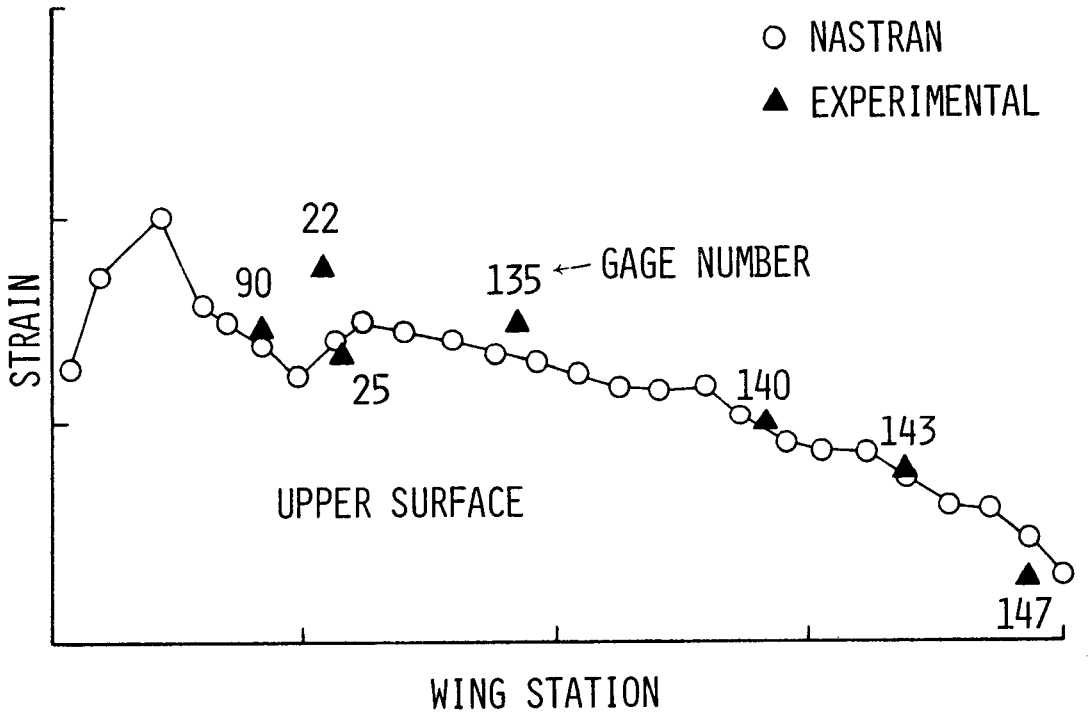

FIGURE 9. STRAINS BETWEEN SPARS 4 & 5 AT ULTIMATE POSITIVE BENDING

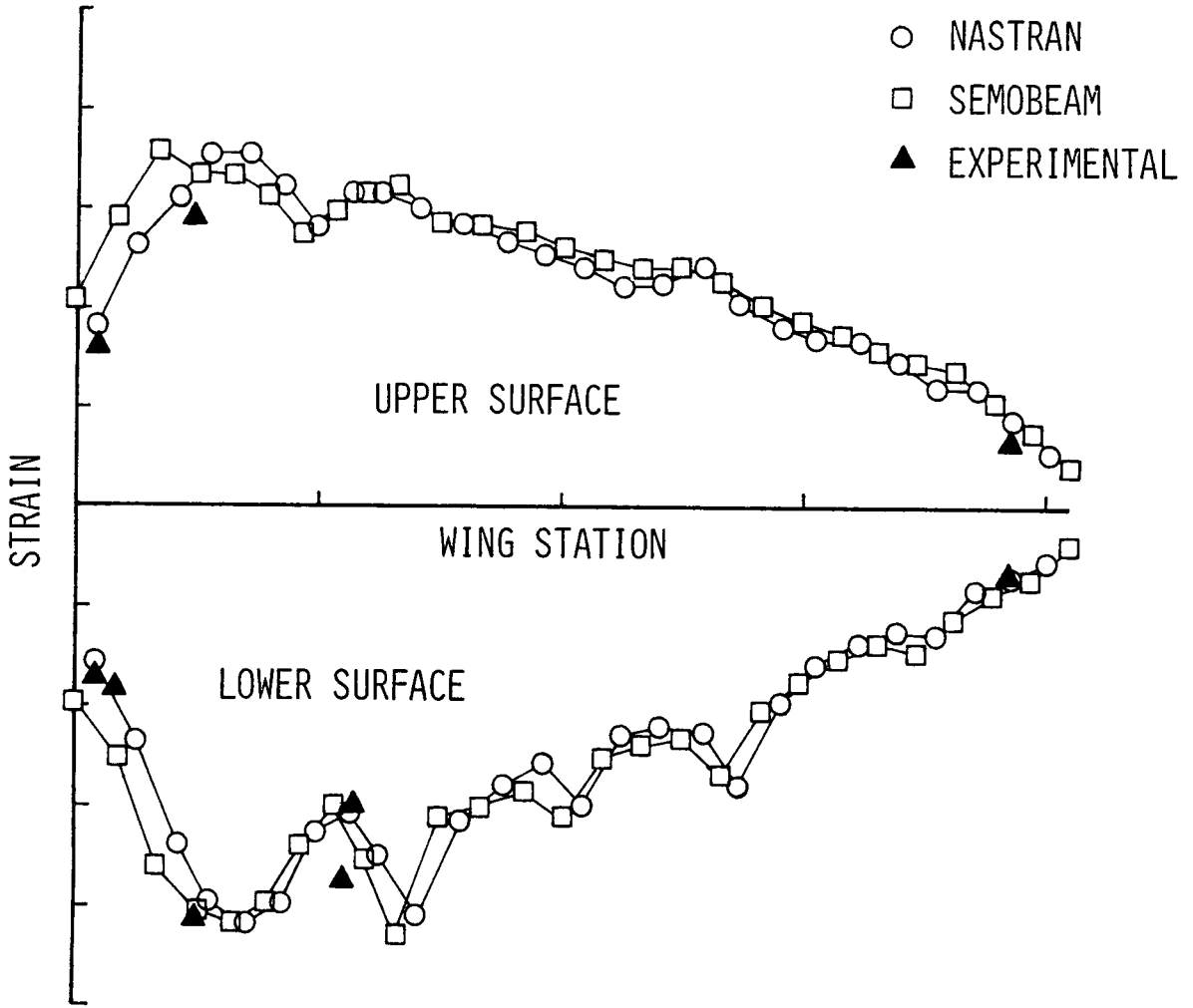

FIGURE 10. SPAR CAP STRAINS IN SPAR 3 AT ULTIMATE POSITIVE BENDING

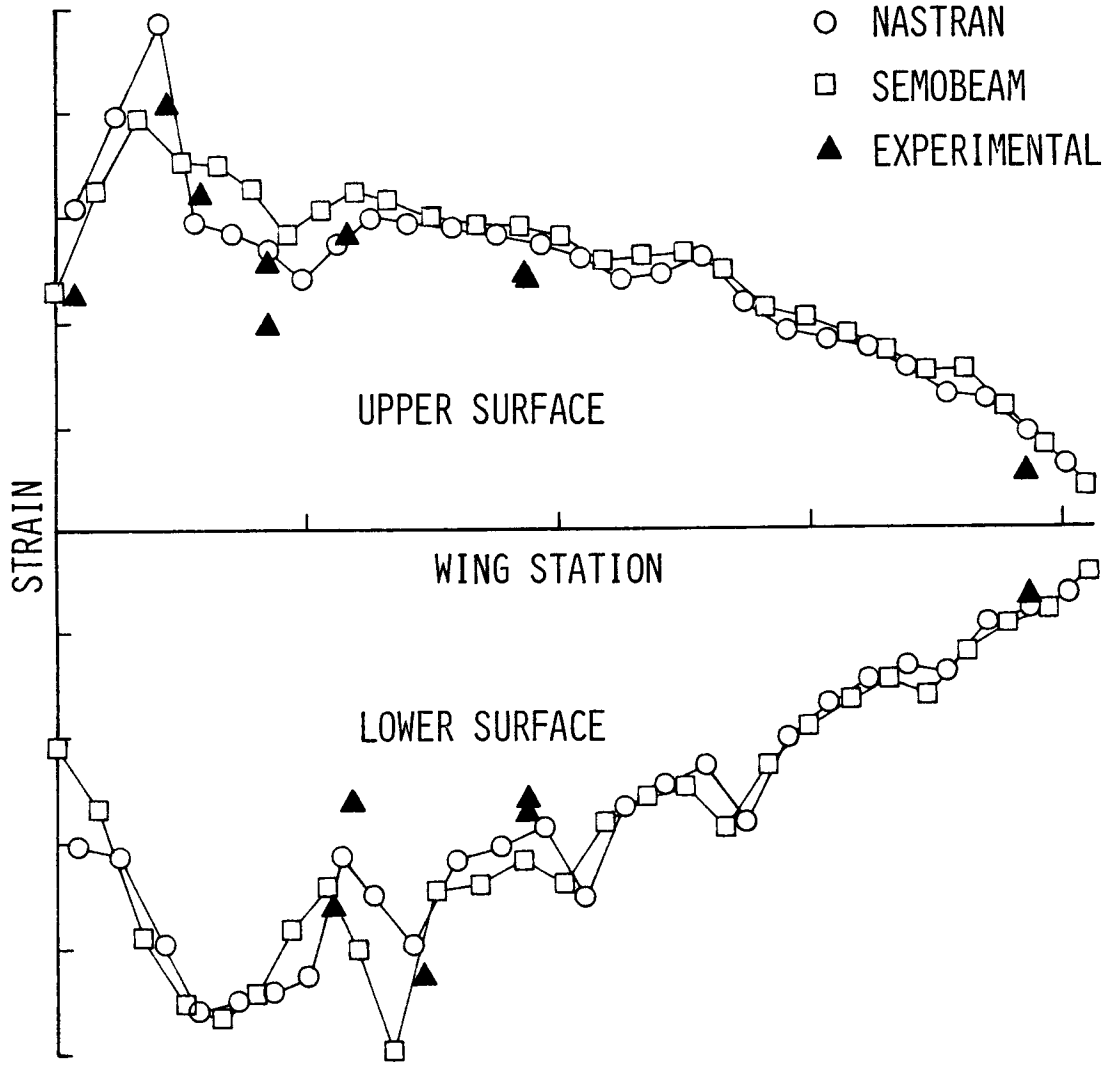

FIGURE 11. SPAR CAP STRAINS IN SPAR 5 AT ULTIMATE POSITIVE BENDING